

## A LOW MACH NUMBER VARIABLE DENSITY LARGE EDDY SIMULATION ALGORITHM FOR TURBULENT BUOYANT FLOWS WITH HEAT TRANSFER

İlyas Yılmaz<sup>a,\*1</sup>, Hasan Saygın<sup>a</sup>, Lars Davidson<sup>b</sup>

<sup>a</sup>Department of Mechanical Engineering, Faculty of Engineering, Istanbul Aydın University, Florya, 34295, Istanbul, Turkey

<sup>b</sup>Division of Fluid Dynamics, Department of Applied Mechanics, Chalmers University of Technology, SE-412 96 Gothenburg, Sweden

\*Correspondence author: Email: [ilyasyilmaz@aydin.edu.tr](mailto:ilyasyilmaz@aydin.edu.tr)

Keywords: Large Eddy Simulation, Heat Transfer, Turbulent Buoyant Flow, Low Mach number, Variable Density

### ABSTRACT

A Large Eddy Simulation algorithm for analyzing buoyancy- and thermally- driven transitional and turbulent flows is presented. The compressible Navier-Stokes Equations are non-dimensionalized using low Mach number scaling. The non-dimensional equations are then Favre filtered. The Sub-grid Scale viscosity and heat flux are modeled via Wall-Adapting Local Eddy-Viscosity model and conventional Eddy-Diffusivity Model respectively. A fully implicit, non-dissipative, discrete kinetic energy conserving method is used for the solution. A finite volume LES solver is developed based on the resulting algorithm and fully parallelized with PETSc library. The linear systems stemming from the implicit discretization are efficiently solved by incomplete LU-preconditioned GMRES. The flow solver is applied to buoyancy-driven flow in Rayleigh-Taylor Instability and thermally-driven flow in turbulent Rayleigh-Bénard Convection. The results obtained are successfully compared with the previous experimental and numerical data. This work shows that low Mach number approximation is physically more accurate and better captures the evolution and complex physics of turbulent buoyant flows with or without heat transfer due to the fact that the effects of density and viscosity changes are properly taken into account. Additionally, it allows to study large temperature differences which are beyond the capability and validity of the incompressible Navier-Stokes equations with Oberbeck-Boussinesq assumption.

### NOMENCLATURE

$\alpha$	growth rate
$\kappa$	thermal diffusivity
$\chi$	local mole fraction
$\rho$	density
$\tau$	characteristic time
$\mu$	dynamic viscosity
$\gamma$	ratio of specific heats
$\theta$	mixing efficiency
$g$	gravity
$h$	penetration length
$l$	length
$p$	pressure
$t$	time
$H$	height
$T$	temperature
$A_0$	amplitude
$Rand$	random value
$u_i$	velocity vector
$x_j$	space vector
$g_{ij}$	velocity gradient tensor
$\tau_{ij}$	stress tensor
$S_{ij}$	strain rate tensor
$\Delta$	grid size
$( )_0$	reference quantity
$( )_{sgs}, ( )^{sgs}$	sub-grid scale quantity
$( \bar{ } )$	spatially filtered
$( \tilde{ } )$	Favre filtered
$( )', ( )''$	sub-grid scale component

<sup>1</sup> Present address: Division of Fluid Dynamics, Department of Applied Mechanics, Chalmers University of Technology, Gothenburg, SE-412 96, Sweden.

## INTRODUCTION

Variable density and temperature effects in turbulent flows at low Mach numbers can be stemming from strong stratification or large temperature differences. Many industrial flows such as flows in heat exchangers or combustion chambers and many natural flows such as free shear flows or stellar atmospheres can subject to density and temperature variations and exhibit challenging behavior for the numerical methods which only applicable to certain range of flow regimes. At that point, low Mach number methods capable of density/temperature changes without suffering from the numerical and physical constraints can provide an efficient way to deal with these flows properly. There is also a fact that relatively less numerical and experimental data available in the literature for low Mach number, variable property turbulent flows.

This study mainly presents some efforts on developing a Large Eddy Simulation (LES) algorithm for this purpose and its applications to flows canonically represent challenging physics mentioned above. In order to perform this study, the governing equations with buoyancy force are made non-dimensional via low Mach number scaling and Favre filtered to obtain the working set of LES equations. An all-speed, non-dissipative, fully implicit, kinetic energy conserving solution procedure proposed by Hou and Mahesh [1] for Direct Numerical Simulation (DNS) of turbulent flows is used for discretization. The Wall-Adapting Local-Eddy (WALE) viscosity Sub-grid Scale (SGS) model [2] for SGS stresses and the eddy-diffusivity hypothesis for SGS heat fluxes are utilized. An implicit, fully parallel LES solver was also developed using the PETSc library [3]. The linear systems arising from the discretization are solved using an efficient, incomplete LU-preconditioned GMRES.

The aim of the present study is twofold; firstly, to present an efficient algorithm for LES which is applicable to low Mach number flows with density/temperature variations and heat transfer, and secondly, to show that this approach can predict the evolution of challenging flows in a physically more accurate way without limitations or relying on any further assumptions.

The outline of the papers is as follows. Section 2 gives the details of the governing equations, the LES filtering and the SGS modeling. The numerical method used for discretization and the flow solver as well will

be mentioned in Section 3. Section 4 presents the results obtained and discusses in detail and the final conclusions are made in the last section.

## LES FORMULATION

The governing equations are the fully compressible Navier-Stokes Equations (NSE) with buoyancy term which read

$$\frac{\partial \rho}{\partial t} + \frac{\partial \rho u_j}{\partial x_j} = 0 \quad (1)$$

$$\frac{\partial \rho u_i}{\partial t} + \frac{\partial \rho u_i u_j}{\partial x_j} = -\frac{\partial p}{\partial x_i} + \frac{\partial \tau_{ij}}{\partial x_j} + \rho g_i \quad (2)$$

$$\frac{\partial \rho E}{\partial t} + \frac{\partial (\rho E + p) u_j}{\partial x_j} = \frac{\partial \tau_{ij} u_i}{\partial x_j} + \frac{\partial q_j}{\partial x_j} + \rho g_i u_i \quad (3)$$

where  $\tau_{ij} = \mu \left( \frac{\partial u_i}{\partial x_j} + \frac{\partial u_j}{\partial x_i} - \frac{2}{3} \frac{\partial u_k}{\partial x_k} \delta_{ij} \right)$  is the stress tensor and  $q_j = -c_p \frac{\mu}{Pr} \frac{\partial T}{\partial x_j}$  is the heat flux. The system is closed with the Equation of State (EOS) for an ideal gas  $p = \rho RT$ .

The non-dimensional form of the equations are obtained using the standard procedure, except for the pressure. The pressure is made non-dimensional in a way that the resulting equations reduce to the incompressible NSE as the Mach number goes to zero. This is known as *low Mach number scaling* and achieved using  $p^{nd} = \frac{p-p_0}{\rho_0 u_0^2}$  [4, 5]. Omitting the non-dimensionality superscript  $\{ \}^{nd}$  for clarity, the non-dimensional set of governing equations are given by

$$\frac{\partial \rho}{\partial t} + \frac{\partial \rho u_j}{\partial x_j} = 0 \quad (4)$$

$$\frac{\partial \rho u_i}{\partial t} + \frac{\partial \rho u_i u_j}{\partial x_j} = -\frac{\partial p}{\partial x_i} + \frac{1}{Re} \frac{\partial \tau_{ij}}{\partial x_j} + \frac{1}{Fr^2} \rho g_i \quad (5)$$

$$\begin{aligned} Mr^2 \left[ \frac{\partial}{\partial t} \left( p + \frac{\gamma-1}{2} \rho u_i u_i \right) + \frac{\partial}{\partial x_j} \left( \gamma p + \frac{\gamma-1}{2} \rho u_i u_i \right) u_j \right] \\ + \frac{\partial u_j}{\partial x_j} = \frac{(\gamma-1) Mr^2}{Re} \frac{\partial \tau_{ij} u_i}{\partial x_j} + \frac{1}{Re} \frac{\partial}{\partial x_j} \left( \frac{\mu}{Pr} \frac{\partial T}{\partial x_j} \right) \\ + \frac{Ec}{Fr^2} (\rho g_i u_i) \end{aligned} \quad (6)$$

$$\rho T = \gamma Mr^2 p + 1 \quad (7)$$

In LES, the large scales are resolved and contributions from the small scales are modeled. In order to obtain the LES equations, a spatial filter is applied. As a natural choice in Finite Volume

Methods (FVM), the grid size is taken as the filter width. The filtered flow field,  $f$ , is decomposed into *the resolved* and *the unresolved* parts,  $f = \bar{f} + f'$ . A density weighting procedure known as Favre filtering is also introduced to simplify the filtered equations for compressible flows via  $\tilde{f} = \overline{\rho f} / \bar{\rho}$ . Now, the decomposition can be re-written as  $f = \tilde{f} + f''$ . Due to the fact that the Mach number of the flows considered here are sufficiently low, it is also possible to neglect some other terms arising from the filtering.

Finally, the Favre filtered equations are obtained as follows

$$\frac{\partial \bar{\rho}}{\partial t} + \frac{\partial \bar{\rho} \tilde{u}_j}{\partial x_j} = 0 \quad (8)$$

$$\frac{\partial \bar{\rho} \tilde{u}_i}{\partial t} + \frac{\partial \bar{\rho} \tilde{u}_i \tilde{u}_j}{\partial x_j} = -\frac{\partial \bar{p}}{\partial x_i} + \frac{1}{Re} \frac{\partial \bar{\tau}_{ij}}{\partial x_j} - \frac{\partial \tau_{ij}^{sgs}}{\partial x_j} + \frac{1}{Fr^2} \bar{\rho} \tilde{g}_i \quad (9)$$

$$\begin{aligned} Mr^2 \left[ \frac{\partial}{\partial t} \left( \bar{p} + \frac{\gamma-1}{2} \bar{\rho} \tilde{u}_i \tilde{u}_i \right) + \frac{\partial}{\partial x_j} \left( \gamma \bar{p} + \frac{\gamma-1}{2} \bar{\rho} \tilde{u}_i \tilde{u}_i \right) \tilde{u}_j \right] \\ + \frac{\partial \tilde{u}_j}{\partial x_j} = (\gamma-1) Mr^2 \left( \frac{1}{Re} \frac{\partial \bar{\tau}_{ij} \tilde{u}_i}{\partial x_j} - \frac{\partial \tau_{ij}^{sgs} \tilde{u}_i}{\partial x_j} \right) \\ + \frac{1}{Re} \frac{\partial}{\partial x_j} \left( \frac{\mu}{Pr} \frac{\partial \tilde{T}}{\partial x_j} \right) - \frac{\partial q_j^{sgs}}{\partial x_j} + \frac{Ec}{Fr^2} (\bar{\rho} \tilde{g}_i \tilde{u}_i) \quad (10) \end{aligned}$$

$$\bar{\rho} \tilde{T} = \gamma Mr^2 \bar{p} + 1 \quad (11)$$

Here,  $\tau_{ij}^{sgs} = \bar{\rho} (\tilde{u}_i \tilde{u}_j - \tilde{u}_i \tilde{u}_j)$  is the SGS stress tensor and  $q_j^{sgs} = \bar{\rho} (\tilde{T} \tilde{u}_j - \tilde{T} \tilde{u}_j)$  is the SGS heat flux. These terms will be modeled to introduce the effects of small scales on the resolved flow. The SGS stress tensor consists of two parts as *the anisotropic* and *the isotropic*  $\tau_{ij}^{sgs} = \tau_{ij}^{sgs,a} + \frac{1}{3} \tau_{kk}^{sgs} \delta_{ij}$ . Usually, the isotropic part is neglected [6] and the anisotropic part is modeled based on the assumption that it is proportional to the filtered strain rate tensor  $\tilde{S}_{ij}$

$$\tau_{ij}^{sgs,a} = -2\mu_{sgs} \left( \tilde{S}_{ij} - \frac{1}{3} \tilde{S}_{kk} \delta_{ij} \right) \quad (12)$$

where  $\tilde{S}_{ij} = \frac{1}{2} \left( \frac{\partial \tilde{u}_i}{\partial x_j} + \frac{\partial \tilde{u}_j}{\partial x_i} \right)$  and  $\mu_{sgs}$  is the SGS eddy-viscosity. This assumption is called the *eddy-viscosity hypothesis*. Similarly, the SGS models based on this hypothesis are called the *eddy-viscosity* models.  $\mu_{sgs}$  is determined either algebraically or solving an additional equation. So, the *eddy-viscosity* models can be further classified as the *zero* and the *one-equation* models.

In this study, the WALE model is chosen as the SGS model. It is an advanced, algebraic *eddy-viscosity* model. It utilizes a differential operator based on the traceless symmetric part of the square of the velocity gradient tensor

$$S_{ij}^d = \frac{1}{2} (\tilde{g}_{ij}^2 + \tilde{g}_{ji}^2) - \frac{1}{3} \tilde{g}_{kk}^2 \delta_{ij} \quad (13)$$

where  $\tilde{g}_{ij}^2 = \tilde{g}_{ik} \tilde{g}_{kj}$  and  $\tilde{g}_{ij} = \frac{\partial \tilde{u}_i}{\partial x_j}$  is the velocity gradient tensor. Then,  $\mu_{sgs}$  is calculated using

$$\mu_{sgs} = \bar{\rho} (C_w \Delta)^2 \frac{(S_{ij}^d S_{ij}^d)^{3/2}}{(\tilde{S}_{ij} \tilde{S}_{ij})^{5/2} + (S_{ij}^d S_{ij}^d)^{5/4}} \quad (14)$$

with  $C_w = 0.334$ .

Due to its advanced operator, the WALE model has better scaling properties in laminar, transitional and turbulent regimes and show correct near-wall behavior without using a damping function.

SGS heat flux is also modeled using the *eddy-diffusivity hypothesis* as

$$q_{ij}^{sgs} = -\frac{\mu_{sgs}}{Pr_{sgs}} \frac{\partial \tilde{T}}{\partial x_j} \quad (15)$$

where  $Pr_{sgs}$  is the SGS Prandtl number set to 0.8.

## NUMERICAL METHODOLOGY

The Favre filtered governing equations are discretized using an advanced, implicit, pressure-correction type, iterative predictor-corrector algorithm proposed by Hou and Mahesh [1]. The algorithm is also non-dissipative and kinetic energy conserving at incompressible limit that make it attractive for LES. It is second-order in both space and time and uses co-located variable storage. The thermodynamic variables are half time step staggered from velocity. The face normal velocities are also treated as a separate variable and updated in time to mimic the staggered grids and to suppress the odd-even pressure decoupling in space. Due to space limitations, the complex derivation and discretization steps will not be given here. The further details can be found in [1]. The algorithm was also modified using an additional correction to pressure in time in order to enhance its convergence characteristics by preventing oscillatory successive pressure corrections as in [7].

The present simulations are performed using an in-house, fully implicit, fully parallel DNS solver, *i*DNS, written with PETSc. *i*DNS uses incomplete LU preconditioned-GMRES to solve the linear systems stemming from the implicit discretization. *i*DNS is based on the mentioned DNS algorithm and previously validated for various transitional and turbulent flows [8-10]. In order to perform this study, it was extended to LES by implementing the WALE SGS model and the SGS heat flux calculation.

## RESULTS AND DISCUSSION

*Rayleigh-Taylor Instability* (RTI) occurs when a heavy fluid of density,  $\rho_h$ , on top is supported against the gravity,  $g$ , by a light fluid of density,  $\rho_l$ , on bottom. When it is subject to perturbations, the flows initially in hydrostatic equilibrium start to interpenetrate each other due to the baroclinic vorticity generated by the opposite density and pressure gradients. It can be observed in flows such as type Ia supernovae, inertial confinement fusion, cavitation bubbles, oceanic/atmospheric currents and many other industrial and natural flows.

Penetration of the light fluid into the heavy one as bubbles and penetration of the heavy fluid into the light one as spikes can be modelled in terms of the penetration lengths using  $h_b = \alpha_b Agt^2$  and  $h_s = -\alpha_s Agt^2$  respectively. The total mixing zone can be defined as  $h = h_b(t) - h_s(t) = \alpha Agt^2$  and the corresponding growth rate is given by  $\dot{h} = 2\alpha Agt$ . Here,  $A = \frac{\rho_h - \rho_l}{\rho_h + \rho_l}$  is the Atwood number and  $\alpha$  is the total growth rate given as the sum of the bubble and the spike growth rates,  $\alpha_b$  and  $\alpha_s$ , respectively.

The flow is initialized with Atwood number 0.5 which corresponds to the density ratio of 3. The fluids are initially at rest with constant downward gravitational acceleration and in hydrostatic equilibrium  $p = p_0 - \rho gy$ .  $p_0$  is the reference pressure. The reference density  $\rho_0$  is the light fluid density. The width of the domain is taken as the reference length  $l_0$ . The reference velocity is the *free-fall velocity* which is found using  $u_0 = \sqrt{gl_0}$ . This leads to the reference time scale  $\tau = \sqrt{\frac{l_0}{Ag}}$ . The Eckert number can be approximated as  $Ec = (\gamma - 1)^2 M_r^2$ . The reference dynamic viscosity  $\mu_0$  here can be calculated using the following grid-dependent relation  $\mu_0 = \omega \sqrt{Ag\Delta^3}$  with  $\omega = 0.21$  [11]. Note that the dynamic viscosity  $\mu$  is

also allowed to change in time and updated using the power-law formula  $\mu = T^n$  with  $n = 0.67$ .

The stream-wise and the span-wise boundary conditions are periodic. The no-slip wall boundary condition is applied to the velocity at top and bottom. The homogeneous Neumann boundary condition for the thermodynamic variables are used at walls.

The domain length is  $H \times 3H \times H$  with a resolution of  $48 \times 144 \times 48$ .  $H$  is set to  $2\pi$ . The interface is located at  $y = 0$ .

Instead of perturbing interface, Jun et.al. [12] showed that perturbing the initial velocity field provides a better way to initialize the instability. Since it does not require smoothing. It is also independent from the resolution and yields identical results. Following this suggestion, the perturbation is added to the vertical velocity component as  $A_0 Rand \left[ 1 + \cos\left(\frac{2\pi}{H}y\right) \right]$ .

The non-dimensional time step is  $1 \times 10^{-3}$ . The simulation was run up to a late non-linear stage where the bubble and spikes reach to walls. The reference Mach number  $M_r = \frac{u_0}{\sqrt{\gamma p_0 / \rho_0}}$  is set to 0.1. The Froude number  $F_r = \frac{u_0}{\sqrt{gl_0}}$  is unity. These choices give the scaling Reynolds number  $Re = \frac{\rho_0 u_0 l_0}{\mu_0}$  as 2240.

Fig. 1 shows the *local mole fraction* iso-surfaces calculated based on the heavy fluid density as

$$\chi(x, y, z, t) = \frac{\bar{\rho}(x, y, z, t) - \rho_l}{\rho_h - \rho_l} \quad (16)$$

The development of the instability in time in terms of penetration of bubbles and spikes is clearly seen. Initially smaller structures evolve into the larger ones in time.

The local mole fraction field is averaged over the homogeneous directions to give mixing zone growth

$$\langle \chi(x, y, z, t) \rangle_{xz} = \frac{1}{NxNz} \sum_{ncells} \chi(x, y, z, t) \quad (17)$$

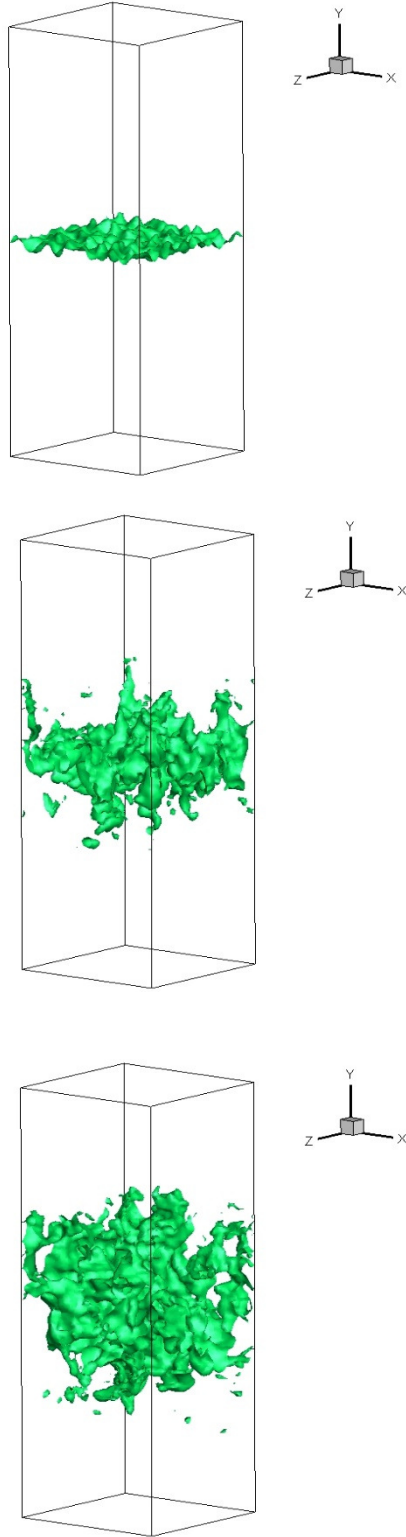


Figure 1

Evolution of the local mole fraction iso-surfaces in time. The non-dimensional time  $t/\tau$  is 3, 6 and 9 from top to bottom respectively

The penetration lengths for bubbles ( $h_b(t)$ ) and spikes ( $h_s(t)$ ) are the distances measured from the interface as  $\langle \chi(x, y, z, t) \rangle_{xz} \leq 1 - \epsilon$  and  $\langle \chi(x, y, z, t) \rangle_{xz} \geq \epsilon$  respectively.  $\epsilon$  is usually set to 0.01.  $h, \dot{h}, \alpha_b, \alpha_s$  and  $\alpha$  then can be easily computed using the relations given above. The penetration lengths and the growth rates are given in Fig. 2. At later times, the spikes penetrate slightly faster than the bubbles with a ratio of  $\sim 1.25$ . The reported numerical and experimental value for  $h_s/h_b$  is in the range of 1.2-1.3 [13-15]. Our result agrees well. At the end of simulation,  $\alpha_b$  reaches a value of  $\sim 0.027$ . Dimonte et. al. [11] and Cook and Dimotakis [15] report values between  $0.02 \leq \alpha_b \leq 0.03$ . The late time value of  $\alpha$  is around 0.061. Again, the reported values of  $\alpha$  are in the range of 0.01-0.07 [14,15]. The results of the current simulation are consistent to those values.

The mixing efficiency  $\theta$  can be computed using

$$\theta = \frac{\int_H \langle \chi(1 - \chi) \rangle_{xz} dy}{\int_H \langle \chi \rangle_{xz} \langle 1 - \chi \rangle_{xz} dy} \quad (18)$$

as in [16].  $\theta$  takes value between 0 and 1 which corresponds to *immiscible* and *complete molecular mixing* case respectively. Fig. 3 plots the mixing efficiency. The final value in our simulation is around 0.82. Cook and Dimotakis [15] and Cook et. al. [17] also report the values around 0.8.

Another problem considered here is the *turbulent Rayleigh-Bénard convection* (RBC). It occurs when a horizontal layer of fluid between plates is heated from below and cooled from above. RBC is a thermally- and buoyancy- driven instability. Although it is a type of thermal convection observed mostly in natural flows, it can also be encountered in many engineering flows such as fire, combustion and nuclear reactors. When the temperature difference  $\Delta T$  is sufficiently large, this leads to high Rayleigh number which is given as  $Ra = \frac{\rho g \beta \Delta T H^3}{\mu \kappa}$  and the instability evolves into the turbulent state.

$Ra 6.3 \times 10^5$  with  $\Delta T = 10^\circ K$  is studied here which corresponds to the *soft turbulent* regime. The initial velocity field is zero everywhere. The initial density and pressure distributions are  $\rho = \rho_0 \left( 1 + \beta \left( \frac{\Delta T}{H} \right) y \right)$  and  $p = p_0 - \rho g y$  respectively.

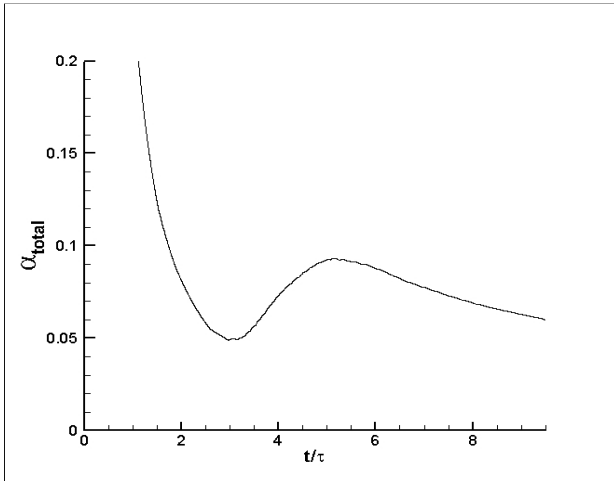
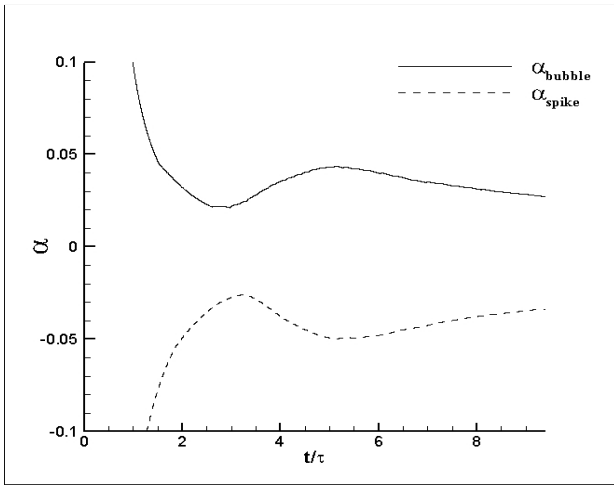
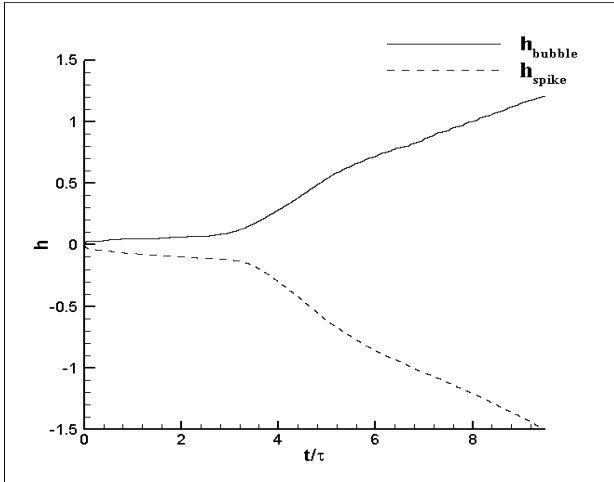


Figure 2

Evolution of the penetration lengths (top), the growth rates (middle) and the total growth rate (bottom) in time

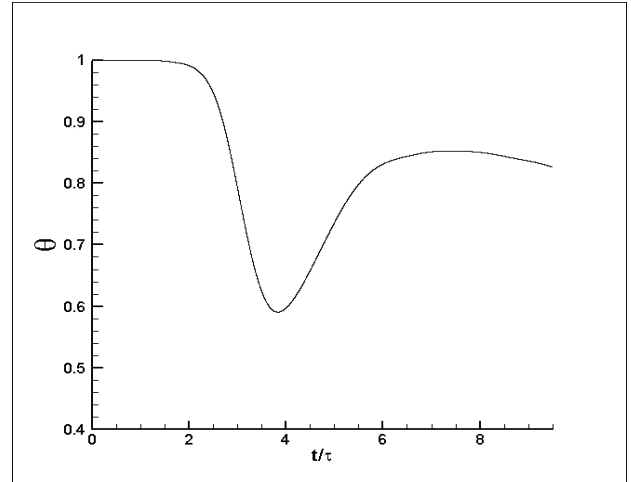


Figure 3

Evolution of the mixing efficiency in time.

Notice that no Oberbeck-Boussinesq (OB) assumption made neither here nor in the governing equations. The non-dimensional temperature and dynamic viscosity at initial and during the simulations are found via the non-dimensional EOS and the power-law.

Top and bottom surfaces are no-slip walls with constant temperatures. The other directions are periodic.

The domain is  $6H \times H \times 6H$  with a resolution of  $64 \times 96 \times 64$ . The domain width  $H$  is taken as the reference length. The reference velocity and the reference time scale are calculated using  $u_0 = \sqrt{g\beta\Delta TH}$  and  $\tau = \frac{H}{u_0}$  respectively. The non-dimensional time step is  $1 \times 10^{-3}$ . The reference Mach number is set to 0.1. It should be noted that, since the ratio of  $\frac{M^2}{dt}$  has strong effect on the diagonally dominance of the discrete form of pressure-correction equation, it can be adjusted properly in order to save the computational time. These choices also give the scaling Reynolds number as approximately 1000.

The simulation was run up to a sufficiently long time to obtain correct statistics which are computed as  $\phi' = \tilde{\phi} - \langle \tilde{\phi} \rangle$  and  $\phi_{rms} = \langle \phi'^2 \rangle^{1/2}$ .

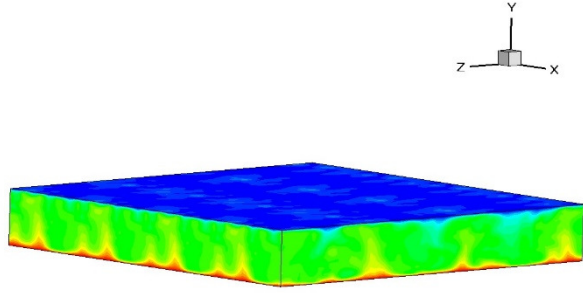


Figure 4

The instantaneous temperature field at  $\frac{t}{\tau} = 1350$

Fig. 4 shows an instantaneous temperature field at non-dimensional time 1350. The large scale coherent flow structures are clearly seen. Fig. 5 plot and compare the average temperature and its *rms*, scaled to between 0 and 1. The both are in agreement with the previous experimental [18] and the DNS [19] data.

To analyze heat transfer characteristics are predicted correctly, the Nusselt number,  $Nu = \frac{\langle v'T' \rangle - \langle \kappa \frac{\partial T}{\partial y} \rangle}{\kappa \frac{\Delta T}{H}}$  is plotted in Fig. 6. It is distributed uniformly along the vertical direction except the boundaries where strong temperature gradients exist. Its integrated value gives  $\sim 7.5$  for this *Ra* number where the DNS by Wörner [19] predicts  $\sim 7.3$ .

The vertical velocity skewness  $S = \frac{\langle v'^3 \rangle}{\langle v'^2 \rangle^{3/2}}$  is also given in Fig. 7 and compared to the DNS data by Moeng and Rotunno [20]. It measures the degree of symmetry of the convective updrafts and downdrafts. Positive values point out tiny strong updrafts surrounded by large weak downdrafts, while negative values point out vice versa. Our result is consistent with the DNS data.

## CONCLUSIONS

In this study, a LES algorithm for low Mach number, variable density, turbulent buoyant flows with heat transfer is developed and applied to RTI and RBC with satisfactory results. The main focus of this work is to show that low Mach number approach with variable density can be used to analyze these types of flows in a physically more accurate way.

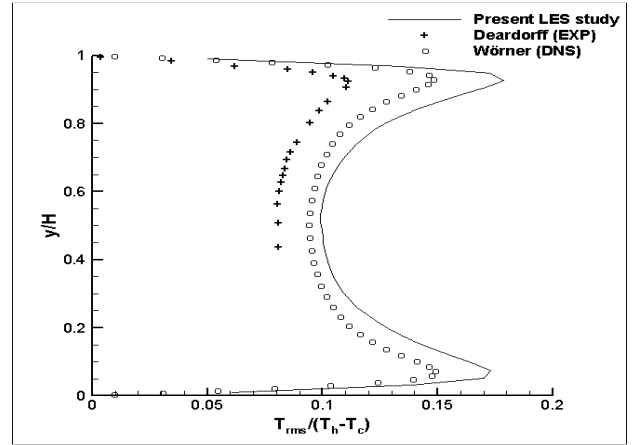
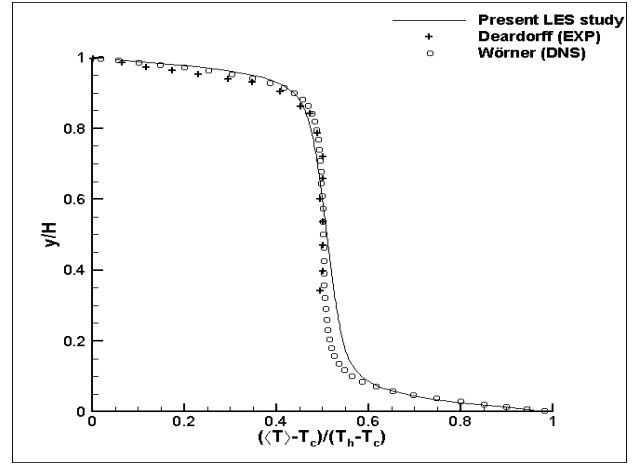


Figure 5

The vertical distribution of average temperature (top) and its *rms* (bottom).

Further flow diagnostics are needed to be incorporated in the future works for better comparisons and understanding.

## ACKNOWLEDGEMENTS

IY thanks to The Scientific and Technological Research Council of Turkey (TUBITAK) for supporting his research stay in Sweden. The computing resources provided by Istanbul Aydin University under the project number BAP2014-04 are gratefully acknowledged.

## REFERENCES

1. Hou, Y., Mahesh, K., 2005, A robust, collocated, implicit algorithm for direct numerical simulation of compressible, turbulent flows, *J. of Comp. Phys.*, **205**, 205–221.

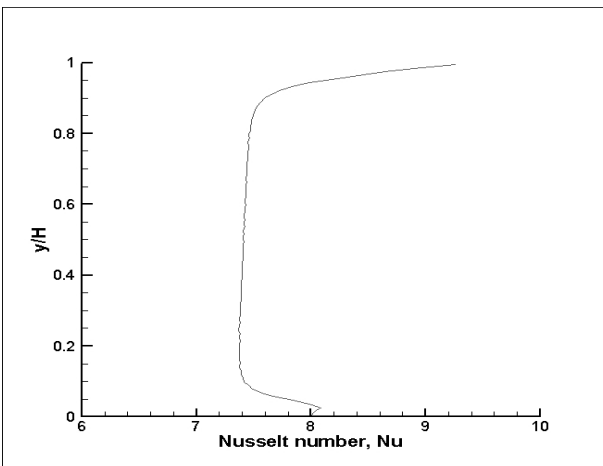


Figure 6

The vertical distribution of Nusselt number

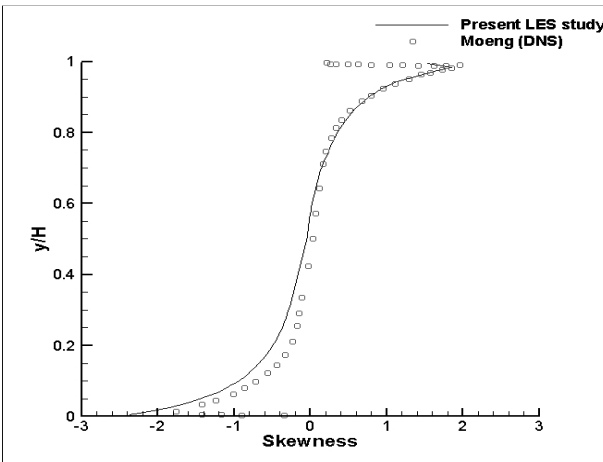


Figure 7

The vertical distribution of skewness

2. Nicoud, F., Ducros, F., 1999, Subgrid-scale stress modelling based on the square of the velocity gradient tensor. *Flow, Turbulence and Combustion*, **62**, pp. 183–200.
3. Balay, S., Gropp, W. D., McInnes, L. C., Smith, B. F., 2014, *PETSc User's Manual*.
4. Panton, R. L., 1984, *Incompressible Flow*.
5. Wesseling, P., 2001, *Principles of Computational Fluid Dynamics*, Springer.
6. Germano, M., Piomelli, U., Moin, P., Cabot, W.H, 1991, A dynamic subgrid-scale eddy viscosity model. *Phy. of Fluids* **A3**, 1760-1765.
7. Walton, G.N., 1989, AIRNET - A Computer Program for Building Airflow Network Modeling, Tech. Report, NISTIR 89-4072.
8. Yilmaz, I., Edis, F. O., Saygin, H., 2014, Application of an all-speed implicit non-dissipative DNS algorithm to hydrodynamic instabilities, *Comp. & Fluids*, **100**, 1,237-254
9. Yilmaz, I., Edis, F.O., Saygin, H., Davidson, L., 2014, Parallel implicit DNS of temporally-evolving turbulent shear layer instability, *J. of Comp. and Appl. Math.*, **259**, 651-659.
10. Yilmaz, I., Edis, F. O., Saygin, H., 2015, Application of an all-speed implicit finite volume algorithm to Rayleigh-Taylor instability, *Int. J. of Comp. Meth.*, 12 (3).
11. Dimonte, G., D.L., Y., et. al., 2004. A comparative study of the turbulent Rayleigh–Taylor instability using high–resolution three–dimensional numerical simulations: The Alpha–Group collaboration, *Phy. of Fluids*, **16**, 1668–1693.
12. Jun, B.I., Norman, M.L. and Stone, J.M., 1995, A Numerical Study of Rayleigh-Taylor Instability in Magnetic Fluids, *Astrophys. J.*, **453**, 332.
13. Read, K., 1984, Experimental investigation of turbulent mixing by Rayleigh-Taylor instability, *Physica D: Nonlinear Phenomena*, **12** (1–3), 45 – 58.
14. Burton, G.C., 2011, Study of ultrahigh Atwood-number Rayleigh–Taylor mixing dynamics using the nonlinear large-eddy simulation method, *Phy. of Fluids*, **23** (4), 045106.
15. Cook, A.W., Dimotakis, P.E., 2001, Transition stages of Rayleigh–Taylor instability between miscible fluids, *J. of Fluid Mech.*, **443**, 69–99.
16. Youngs, D., 1991, Three-dimensional numerical simulation of turbulent mixing by Rayleigh–Taylor instability, *Phy. of Fluids*, **A3**, 1312–1320.
17. Cook, A.W., Cabot, W., Miller, P., 2004, The mixing transition in Rayleigh–Taylor instability, *J. of Fluid Mech.*, **511**, 333–362.
18. Deardorff, J.W., Willis, G.E., 1967, Investigation of Turbulent Thermal Convection between Horizontal Plates *J. Fluid Mech.*, 28:675-704.
19. Wörner, M., 1994, Direkte Simulation Turbulenter Rayleigh-Bénard Konvektion in Flüssigem Natrium,, Dissertation.
20. Moeng, C.H., Rotunno, R., 1990, Vertical-velocity skewness in the buoyancy-driven boundary-layer. *J. Atm. Sci.*, 47, 1149-1162.